PERGAMON

International Journal of Solids and Structures 39 (2002) 4013–4025

INTERNATIONAL JOURNAL OF SOLIDS and STRUCTURES

www.elsevier.com/locate/ijsolstr

Damage constitutive for high strength concrete in triaxial cyclic compression

Qingbin Li [a,*], Lixiang Zhang [b], Farhad Ansari [c]

[a] *Department of Hydraulic Engineering, Tsinghua University, Beijing 100084, China*

[b] *Department of Hydraulic Engineering, Kunming University of Science and Technology, Kunming 650051, China*

[c] *Department of Civil & Materials Engineering, University of Illinois at Chicago, 842 W. Taylor St., Chicago, IL 60607-7023, USA*

Received 10 October 2001; received in revised form 22 March 2002

Abstract

A constitutive relationship for high strength concrete in triaxial monotonic and cyclic compressions is developed based on the continuum damage mechanics. The bounding surface concept is employed in the formulation of the theoretical model. An experimental program was undertaken in order to establish databases for high strength concrete under triaxial monotonic and cyclic compressions. The stress-strain responses of high strength concrete subjected to triaxial monotonic and cyclic compressions were acquired through an experimental program. Comparison of the stress strain results indicates good agreement between the theoretical model and the experimental data.

Keywords: High strength concrete; Triaxial compression; Monotonic; Cyclic; Damage; Bounding surface; Basic surface; Threshold damage surface; Load path; Constitutive relationship; Experiments

1. Introduction

Constitutive relationships for normal strength concrete in monotonic and cyclic compression (uniaxial and biaxial) have been developed in many publications (Fafitis and Shah, 1986). Employment of continuum damage mechanics for development of constitutive relationships stems from the fact that the damage-mechanics-based models have been able to accurately account for the microcracking and softening behavior of concrete (Krajcinovic and Selvaraj, 1983; Mazars and Cabot, 1989). Theories based purely on the theory of plasticity pertain to materials exhibiting strains as a consequence of slip in their shear planes. Damage in concrete is associated with progressive evolution and nucleation of microcracks. This invalidates formulation of theories that are solely based on plasticity models. A survey of the technical literature yields a number of damage-based theories for normal strength concrete. Early work pertained to the quantification of damage in terms of vectors and tensors (Krajcinovic and Fonseka, 1981; Ortiz, 1985). Chow and Wang

* Corresponding author. Tel.: +86-10-6277-1015; fax: +86-10-6278-5699.
E-mail address: qingbli@hotmail.com (Q. Li).

0020-7683/02/$ - see front matter
PII: S0020-7683(02)00265-2

(1987) developed the underlying mathematical framework for the general case of anisotropic damage. Fardis et al. (1983) proposed a bounding surface concept for damage in concrete based on the principles previously employed in conjunction with metallic materials (Dafalias, 1986). Based on physical evidence, Voyiadjis and Abu-Lebdeh (1993) realized that the kinematics of damage in tension and in compression are governed by different sets of variables. By using the bounding surface concept they were able to characterize damage accurately and develop corresponding constitutive relationships for concrete. Such theories have not yet been developed for high strength concrete, in cyclic loading (Li and Ansari, 1999). Accordingly, the objective of the work presented here is to establish an accurate constitutive relationship for high strength concrete in triaxial monotonic and cyclic compressions.

2. Failure surface

The failure surface for high strength concrete was developed by least square fit of the experimental data to the four parameter constitutive model of Ottosen (1977) in Ansari and Li (1998). The coordinate system and the deviatoric plane shown in Fig. 1 can be used for defining the various elements of the failure surface. For this purpose, any point $P(\sigma_1, \sigma_2, \sigma_3)$ in the stress space is described by the coordinates (ξ, ρ, θ) in which ξ is the projection on the hydrostatic axis, and (ρ, θ) are polar coordinates in the deviatoric plane which is orthogonal to the hydrostatic axis. Compressive stresses are considered positive, The failure surface can be completely described by the compressive ($\theta = 0°$, $\sigma_1 = \sigma_2 < \sigma_3$) and the tensile ($\theta = 60°$, $\sigma_1 = \sigma_2 > \sigma_3$) meridians.

The failure criterion can be described in terms of the invariants in the following form:

$$F(\sigma_{ij}) = A\frac{J_2}{(f'_c)^2} + \lambda\frac{\sqrt{J_2}}{f'_c} - B\frac{I_1}{f'_c} - 1 = 0, \tag{1}$$

where,

$$\lambda = k_1 + k_2\cos 3\theta, \tag{2}$$

$$\cos 3\theta = \frac{3\sqrt{3}}{2}\frac{J_3}{J_2^{3/2}}. \tag{3}$$

F is the failure function, i.e. $F(\sigma_{ij}) < 0$ corresponds to the stress states inside the failure surface, or $F(\sigma_{ij}) = 0$, and $(\mathrm{d}f/\mathrm{d}\sigma)(I_1, J_2, \cos 3\theta) \geqslant 0$ corresponds to the failure state. I_1 is the first invariant of the stress tensor, J_2 and J_3 pertain to the deviatoric principal stress invariants, i.e.:

$$I_1 = \sigma_1 + \sigma_2 + \sigma_3 = \sigma_{ii}, \tag{4}$$

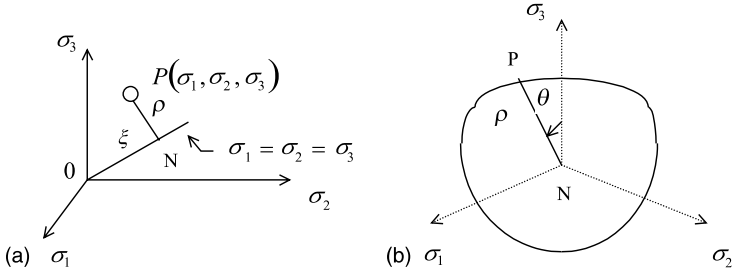

Fig. 1. (a) Haigh-Westergaard coordinate system and (b) deviatoric plane.

$$J_2 = \tfrac{1}{2}\left(s_1^2 + s_2^2 + s_3^2\right) = \tfrac{1}{2}s_{ij}s_{ij}, \tag{5}$$

$$J_3 = \tfrac{1}{3}\left(s_1^3 + s_2^3 + s_3^3\right) = \tfrac{1}{3}s_{ij}s_{jk}s_{ki}. \tag{6}$$

σ_{ij} is the stress tensor, and s_{ij} is the stress deviator tensor (i.e., $s_{ij} = \sigma_{ij} - (1/3)\delta_{ij}\sigma_{kk}$). The hydrostatic and deviatoric planes are represented by:

$$\xi = \frac{I_1}{\sqrt{3}}, \tag{7a}$$

$$\rho = \sqrt{2J_2}. \tag{7b}$$

ξ and ρ can be used for defining the failure surface in terms of the compressive and tensile meridians. A, B, k_1, and k_2 are the four parameters in the failure criterion that were determined in Ansari and Li (1998).

3. Theoretical analysis

In this section, theoretical formulations are presented based on the bounding surface damage theory leading to the development of constitutive relationships for high strength concrete. The damage bounding surface concept stems from the idea that for concrete at a given level of damage, the monotonic and cyclic failure stresses coincide. This implies that both the monotonic and cyclic loading states share a unique innermost envelope in the stress space. From which both loading types depend for higher loadings. The onset of damage is described by an initial surface indicating the damage threshold limit for the material. The bounding surface pertains to the failure state of the material. The position of the loading surface in the stress space between the initial and the bounding surfaces describe the various levels of damage states. However, the material is considered undamaged when the loading surface lies inside the initial fracture surface.

3.1. Bounding surface damage concept for high strength concrete

The failure surface of normal strength concrete was employed in the development of the damage bounding surface concept for normal strength concrete (Voyiadjis and Abu-Lebdeh, 1993). The experimental works of Karsan and Jirsa (1969), Cedolin et al. (1977), Buyukozturk and Tseng (1984), Kosovos and Newman (1980), and Kupfer et al. (1969) have been considered for the development of the failure criterion. In the present work, the failure surface for high strength concrete (Eq. (1)) is modified to include the effect of damage both for monotonic as well as cyclic loading conditions. Accordingly, the damage bounding surface is described by the function F which is a function of stress state σ_{ij} as:

$$F(\sigma_{ij}, \overline{D}) = A\frac{J_2}{\left(f'_c\right)^2} + \lambda\frac{\sqrt{J_2}}{f'_c} + B\frac{I_1}{f'_c} - g(\overline{D}) = 0. \tag{8}$$

In which $g(\overline{D})$ is a function related to damage. The damage parameter $\overline{D}$ represents the accumulated damage experienced by the material at each level of evolution. Experimental results were employed for the construction of the damage surfaces in the orthotropic plane (Fig. 2). The bounding surface encloses all the loading surfaces. In Fig. 2, $\beta = f'_t/f'_c$, σ_c^0 is the damage threshold stress in uniaxial compression, and σ_t^0 is the damage threshold stress in uniaxial tension. The meridians of the initial damage surface are closed, They consist of three distinct zones: (1) tension zone, in which the damage threshold surface ($f_0 = 0$) nears the bounding surface, representing brittle behavior of high strength concrete; (2) tension–compression zone, in which the hardening zone gradually increases; (3) high confining compression zone, in which the damage

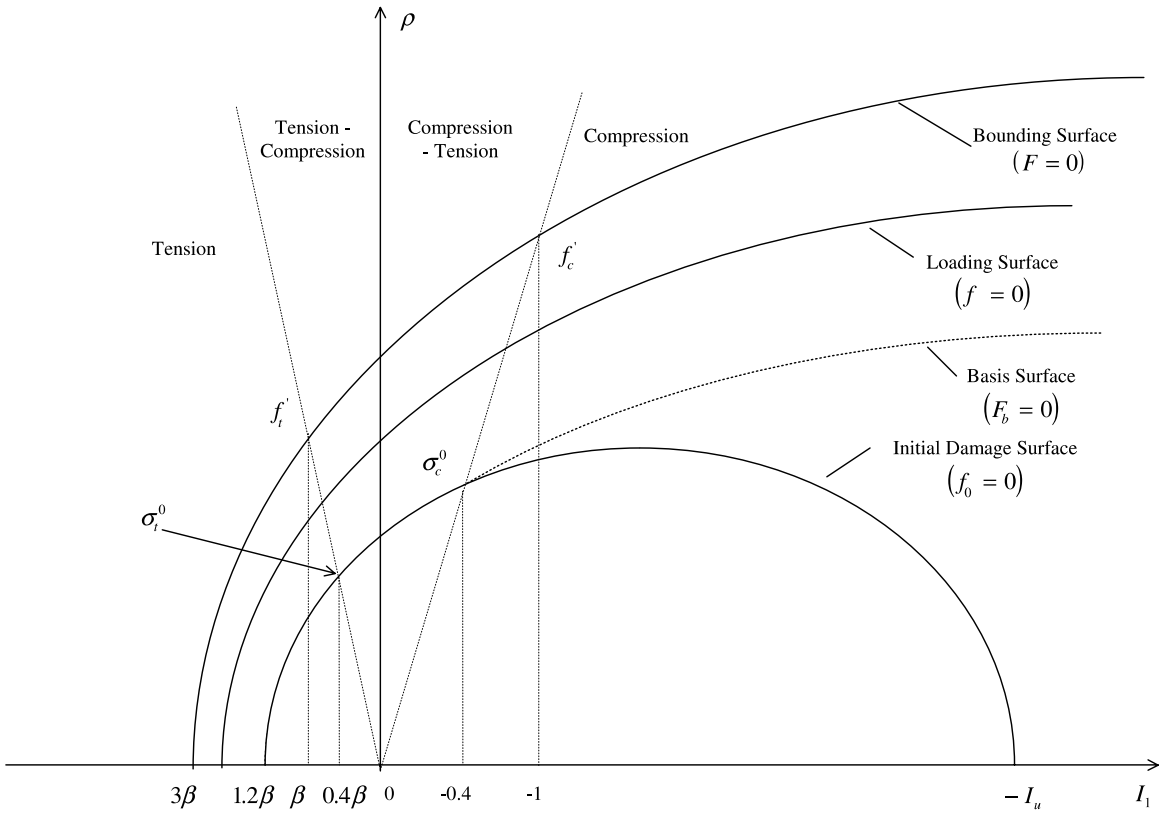

Fig. 2. Construction of bounding, loading, basic, and threshold damage surface.

threshold surface starts to close up producing a large hardening zone. However, once the loading has surpassed the initial damage surface, both the size and the shape of the loading surfaces ($f = 0$) vary from the closed to the final shape (bounding surface). According to the nonuniform hardening rule (Desai and Siriwardance, 1984), each loading surface can be characterized by a shape factor K and expressed in the form:

$$f(\sigma_{ij}, \overline{D}) = A\frac{J_2}{(f_c')^2} + K\lambda\frac{\sqrt{J_2}}{f_c'} + K^2B\frac{I_1}{f_c'} - K^2 g(\overline{D}) = 0. \tag{9}$$

The initial damage surface is expressed in the following form:

$$f(\sigma_{ij}, \overline{D}) = A\frac{J_2}{(f_c')^2} + K\lambda\frac{\sqrt{J_2}}{f_c'} + K^2B\frac{I_1}{f_c'} - K^2\left(1 + \frac{\overline{D}_0}{60}\right) = 0, \tag{10}$$

where, $\overline{D}_0$ is the accumulated damage ($\overline{D}$) at the beginning of any cycle. It should be noted that when $\overline{D}_0 = 0$, Eq. (10) reduces to the initial damage surface in monotonic loading. The shape factor K is assumed to be a function of the hydrostatic stress I_1 and the hardening parameter K_0. According to the experimental results presented here the functional dependence of the damage growth rate on the separation between the loading surface and the bounding surface controls the damage growth of concrete.

The functional form of K is derived on the basis of a nonuniform hardening rule taking into consideration the basic shape requirements for the initial damage surface as well as the subsequent loading surface

on the meridian plane. This is implemented by introducing the basis surface ($F_B = 0$) which has no physical meaning, yet it is useful in formulating the initial damage surface. The basis surface does not intersect the negative hydrostatic axis. It is given in the following format:

$$F_B(\sigma_{ij}) = A\frac{J_2}{(f'_c)^2} + K_B\lambda\frac{\sqrt{J_2}}{f'_c} + K_B^2 B\frac{I_1}{f'_c} - K_B^2 = 0, \tag{11}$$

where, $K_B = \bar{\sigma}_t/f'_t$, is the hardening parameter for the basis surface. $\bar{\sigma}_t$ is the equivalent stress in tension and the root of Eq. (11), i.e.:

$$\bar{\sigma}_t = \frac{-\lambda - \sqrt{\lambda^2 - 4A(BI_1 - 1)}}{2(BI_1 - 1)}\sqrt{J_2}. \tag{12}$$

The shape factor is a function of I_1 and the hardening parameter K_0. Based on the experimental results shown in Fig. 2, K varies, its value depends on the loading as:

$$K = K_B, \quad -I_g \leqslant I_1 \leqslant 3\beta, \tag{13}$$

$$K = K_0(aI_1^2 + bI_1 + c), \quad -I_g \leqslant I_1 \leqslant I_u, \tag{14}$$

where,

$$I_g = \frac{\bar{\sigma}_c}{f'_c}. \tag{15}$$

In which, $\bar{\sigma}_c$ is the equivalent stress in compression that has the same form as Eq. (12), I_u is the intersection of the loading surface with the negative hydrostatic axis, and f'_t is the tensile strength of concrete. I_u corresponds to the effect of confining pressure on the axial strength and is empirically determined from the experimental results as:

$$I_u = \frac{2.8}{1 - K_0}. \tag{16}$$

I_u approaches infinity as the loading surface nears the bounding surface, i.e., $K_0 \to 1$. The hardening parameter K_0 has a value between K_i and 1, where K_i indicates the hardening level of the initial damage surface, and $K_0 = 1$ indicates that the loading surface has reached the bounding surface, so that failure occurs. K_0 is empirically determined from the uniaxial properties of the high strength and is given as:

$$K_0 = 1 - 0.6\left(\frac{E}{E_0}\right)^2, \tag{17a}$$

where, E_0 is the initial Young's modulus (normalized with respect to the uniaxial compressive strength), E is the tangent modulus (normalized with respect to the uniaxial compressive strength), and it is:

$$E = \frac{E_0}{\sqrt{0.6}}\sqrt{1 - \frac{\bar{\sigma}}{f'_c}}. \tag{17b}$$

The function K in Eq. (14) is assumed to be quadratic in I_1 satisfying the shape requirements:

$$\begin{cases} K = K_B, & I_1 = -I_g, \\ K = K_0, & I_1 = -1, \\ K = 0, & I_1 = -I_u. \end{cases} \tag{18}$$

From Eq. (18) one obtains the parameters in Eq. (14) as follows:

$$\begin{cases} a = \frac{(1-I_g)-(1-I_u)(1-K_B/K_0)}{(1-I_u)\cdot(1-I_g)\cdot(I_u-I_g)}, \\ b = \frac{(1-I_u^2)a-1}{1-I_u}, \\ c = 1-a+b. \end{cases} \tag{19}$$

3.2. Evaluation of damage

Previous investigators employed experimental evidence in order to distinguish the damage characteristics of normal strength concrete in terms of tensile and compressive stress states. While some investigators suggested averaging of the tensile and compressive damages in the formulation of damage function (Mazars, 1986), others derived separate relationships for the two states of stress (Voyiadjis and Abu-Lebdeh, 1993). Experimental evidence was used to justify the separation of tensile and compressive modes of cracking. Tensile cracks are created by direct extension, whereas in compression the crack extensions are perpendicular to the direction of applied stress. Accordingly, different damage loading surfaces are needed to consider the growth of damage due to tension D_t, and that of the compression D_c. The present study employs this same approach for characterization of damage in high strength concrete. To implement this, the stress tensor is decomposed into a positive and a negative (compression) tensor σ^+ and σ^- respectively such that:

$$\sigma = \sigma^+ + \sigma^- \tag{20}$$

and

$$\operatorname{tr}\sigma = \operatorname{tr}\sigma^+ + \operatorname{tr}\sigma^-, \tag{21}$$

where σ^+ is built with the positive eigenvalues which appear only in positive principal stresses. It can be obtained by removing the eigensystem associated with negative eigenvalues from σ, whereas, σ^- is built with the negative eigenvalues which appear only in the negative principal stresses. Damage can be tensile, compressive or a combination of the two in complex loading situations. The loading surface, Eq. (9), can be expressed by using separate expressions for the tensile and compressive damage as:

$$f_l = AJ_{2(l)} + \lambda K\sqrt{J_{2(l)}} + K^2BI_{1(l)} - K^2 g_{(l)}(\overline{D}) = 0, \quad l = \mathrm{t}, \mathrm{c}, \tag{22}$$

for tensile damage, $l = \mathrm{t}$ and:

$$J_{2(l)} = J_2^+,$$

$$I_{1(l)} = I_1^+,$$

$$g_l(\overline{D}) = 1 + \overline{D}_t,$$

$$\overline{D}_t = \sqrt{D_{1t}^2 + D_{2t}^2 + D_{3t}^2},$$

for compressive damage, $l = \mathrm{c}$ and therefore:

$$J_{2(l)} = J_2^-,$$

$$I_{1(l)} = I_1^-,$$

$$g_l(\overline{D}) = 1 + \frac{\overline{D}_c}{20},$$

$$\overline{D}_{\mathrm{c}} = \sqrt{D_{1\mathrm{c}}^2 + D_{2\mathrm{c}}^2 + D_{3\mathrm{c}}^2},$$

where, $\overline{D}_{\mathrm{t}}$ and $\overline{D}_{\mathrm{c}}$ are parameters related to the damage principal values of damage tensor. $(D_{1\mathrm{t}}, D_{2\mathrm{t}}, D_{3\mathrm{t}})$ and $(D_{1\mathrm{c}}, D_{2\mathrm{c}}, D_{3\mathrm{c}})$ are the principal values of damage tensor in tension and compression respectively. Accordingly, the damage growth rates in tension and compression grow independent of each other. In terms of the individual flow rules they are evaluated as:

$$\left(\dot{D}_{ij}\right) = \dot{L}\frac{\partial f_l}{\partial \sigma_{ij}}, \tag{23}$$

where the subscript l is interchanged with t, or c for tension and compression as they pertain. In Eq. (23) $\dot{L}$ is the projection of the stress rate $\dot{\sigma}_{ij}$ onto the direction of the normal to the loading surface $\partial f_l/\partial\sigma_{ij}$. Hence:

$$\dot{L} = \frac{1}{h}\frac{\partial f_l\left(\sigma_{ij}, \overline{D}\right)}{\partial \sigma_{mn}}\dot{\sigma}_{mn}, \tag{24}$$

where h is the damage modulus and will be defined later. Substitution of Eq. (24) into Eq. (23) yields the damage growth rate:

$$\left(\dot{D}_{ij}\right)_l = \frac{1}{h_l}\frac{\partial f_l}{\partial \sigma_{ij}}\frac{\partial f_l}{\partial \sigma_{mn}}\dot{\sigma}_{mn}; \quad l = \mathrm{t}, \mathrm{c}. \tag{25}$$

Evaluation of Eq. (25) involves differentiation of the loading surface (22), with respect to stress, σ_{ij}:

$$\frac{\partial f_l}{\partial \sigma_{ij}} = A\frac{\partial J_{(l)}}{\partial \sigma_{ij}} + \lambda\frac{\partial K}{\partial \sigma_{ij}}\sqrt{J_{2(l)}} + \lambda K\frac{1}{2\sqrt{J_{2(l)}}}\frac{\partial J_{2(l)}}{\partial \sigma_{ij}} + BK^2\frac{\partial I_{1(l)}}{\partial \sigma_{ij}} - 2BK\frac{\partial K}{\partial \sigma_{ij}}I_{1(l)} - 2K\frac{\partial K}{\partial \sigma_{ij}}g_{(l)}\left(\overline{D}\right) \tag{26}$$

or

$$\frac{\partial f_l}{\partial \sigma_{ij}} = M_l s_{ij} + N_l \delta_{ij}, \tag{27}$$

where, δ_{ij} is the Kronecker delta,

$$M_l = A + \lambda K\frac{1}{2\sqrt{J_{2(l)}}}, \tag{28a}$$

$$N_l = \lambda\sqrt{J_{2(l)}} + BK^2 - 2K\left(BI_{1(l)} + g_{(l)}\left(\overline{D}\right)\right)\bar{\alpha}. \tag{28b}$$

In which

$$\bar{\alpha} = \begin{cases} \frac{\sqrt{2}}{\sigma_{\mathrm{t}} f_{\mathrm{t}}'}\sigma_{ij}; & -I_{\mathrm{g}} \leqslant I_1 \leqslant 3\beta, \\ K_0(2aI_1 + b); & -I_{\mathrm{u}} \leqslant I_1 \leqslant -I_{\mathrm{g}}. \end{cases} \tag{28c}$$

Substitution of Eq. (27) into Eq. (25) yields the damage growth rate as:

$$\left(\dot{D}_{ij}\right)_l = \frac{1}{h_l}\left[M_{(l)}^2 s_{ij}s_{mn}\dot{\sigma}_{mn} + N_{(l)}^2\delta_{ij}\dot{\sigma}_{mn} + M_{(l)}N_{(l)}\left(\delta_{ij}s_{mn}\dot{\sigma}_{mn} + s_{ij}\dot{\sigma}_{mn}\right)\right]. \tag{29}$$

The damage modulus h is expressed in terms of the distance δ connecting a stress point on the loading surface and the corresponding point on the hydrostatic line. The damage modulus should have the following properties:

1. Within and on the initial damage surface, i.e., $(\delta_{\text{in}} - \delta) \geqslant 0$ the damage modulus is infinite. At this stage, when the loading surface is inside the initial damage surface $(\delta < \delta_{\text{in}})$ damage growth would not occur.
2. Beyond the initial damage surface, the damage modulus h decreases with the distance, δ. When the loading surface approaches the bounding surface the damage modulus reduces to zero causing the failure.

The damage modulus expressions h_{t} and h_{c} (for tension and compression) are derived from the experimental results, and conform with the properties outlined above:

$$h_{\text{t}} = 0.075E_0I_1\left(\frac{1}{\langle \delta^+ - \delta^+_{\text{in}} \rangle}\right)^{2.03}, \tag{30a}$$

$$h_{\text{c}} = 0.045E_0I_1\left(\frac{1}{\langle \delta^- - \delta^-_{\text{in}} \rangle}\right)^{2.03}, \tag{30b}$$

where, $\langle\rangle$ is the Heaviside function; δ^+, δ^- are the normalized distances from the points on the loading surface (in tension and compression) to the hydrostatic line respectively; δ^+_{in}, δ^-_{in} are the normalized distances from the points on the initial damage surface in tension and compression to the hydrostatic line respectively.

Concrete exhibits softening. Considering that it is plastically stable, softening is solely attributed to the evolution of damage. Softening is modeled by computing the damage modulus (h) on the basis that the stress point moves on the bounding surface. The damage modulus is evaluated from the consistency condition of the bounding surface ($\bar{F}$) as:

$$\bar{h}_l = -q_l \frac{1}{\overline{D}} D_{ij} \frac{\partial F}{\partial \overline{D}} \frac{\partial f}{\partial \sigma_{ij}}, \tag{31}$$

where, $\bar{h}_l$ is the damage modulus at bounding surface (i.e., softening modulus), $l = \text{c, t}$; $q_{\text{c}} = 0.002E_0I_1$; and $q_{\text{t}} = 0.000029(E_0/I_1)$; are empirical correction factors; and $\partial F/\partial \overline{D} = g'(\overline{D})$.

3.3. Constitutive relationships

The strain tensor for high strength concrete is derived from the complementary free-energy function in terms of the hydrostatic stress I_1, the deviator stress tensor s_{ij}, damage tensor D_{ij} in the following form:

$$\mathrm{d}\varepsilon_{ij} = \frac{\partial \varepsilon_{ij}}{\partial I_1}\mathrm{d}I_1 + \frac{\partial \varepsilon_{ij}}{\partial s_{kl}}\mathrm{d}s_{kl} + \frac{\partial \varepsilon_{ij}}{\partial D_{kl}}\mathrm{d}D_{kl}. \tag{32}$$

Due to the fact that the stress tensor is separated into its positive and negative eigenvalues, the strain tensor is presented in a likewise manner in the following format:

$$\mathrm{d}\varepsilon_{ij} = C_h\,\mathrm{d}I_1\delta_{ij} + C_{ijkl}\,\mathrm{d}s_{kl} + \mathrm{d}C^{\text{I}}_{ijkl}s^+_{kl} + \mathrm{d}C^{\text{II}}_{ijkl}s^-_{kl}, \tag{33}$$

where C^{I}_{ijkl} is the compliance tensor corresponding to tensile stresses; C^{II}_{ijkl} is the compliance tensor corresponding to compressive stresses. They are determined by decomposition of the compliance tensor as:

$$C_{ijkl} = C^{\text{I}}_{ijkl} + C^{\text{II}}_{ijkl}, \tag{34a}$$

$$\mathrm{d}C^{\text{I}}_{ijkl} = \frac{\partial C^{\text{I}}_{ijkl}}{\partial D_{mn}}\mathrm{d}D_{mn}, \tag{34b}$$

$$\mathrm{d}C^{\mathrm{II}}_{ijkl} = \frac{\partial C^{\mathrm{II}}_{ijkl}}{\partial D_{mn}}\mathrm{d}D_{mn}, \tag{34c}$$

C_h is the bulk compliance. All the compliance tensors are determined from the present experimental results as presented in the following:

$$C_h = \frac{1}{3}\frac{3(1-2v)}{E_0}, \tag{35a}$$

$$[C^{\mathrm{I}}] = \frac{1}{E_0}\begin{bmatrix} \frac{1}{(1-\alpha D_{11})} & -v & -v \\ & \frac{1}{(1-\alpha D_{22})} & -v \\ \text{symmetric} & & \frac{1}{(1-\alpha D_{33})} \end{bmatrix}, \tag{35b}$$

$$[C^{\mathrm{II}}] = \frac{1}{E_0}\begin{bmatrix} \frac{1}{(1-\gamma D_{11})} & -v & -v \\ & \frac{1}{(1-\gamma D_{22})} & -v \\ \text{symmetric} & & \frac{1}{(1-\gamma D_{33})} \end{bmatrix}. \tag{35c}$$

The rate compliance matrices for tensile and compressive stresses $\mathrm{d}C^{\mathrm{I}}$ and $\mathrm{d}C^{\mathrm{II}}$ are derived from Eqs. (35b) and (35c) as:

$$[\mathrm{d}C^{\mathrm{I}}] = \begin{bmatrix} \frac{\mathrm{d}D_{11}}{(1-\alpha D_{11})^2} & 0 & 0 \\ & \frac{\mathrm{d}D_{22}}{(1-\alpha D_{22})^2} & 0 \\ \text{symmetric} & & \frac{\mathrm{d}D_{11}}{(1-\alpha D_{33})^2} \end{bmatrix}, \tag{36a}$$

$$[\mathrm{d}C^{\mathrm{II}}] = \begin{bmatrix} \frac{\mathrm{d}D_{11}}{(1-\gamma D_{11})^2} & 0 & 0 \\ & \frac{\mathrm{d}D_{22}}{(1-\gamma D_{22})^2} & 0 \\ \text{symmetric} & & \frac{\mathrm{d}D_{11}}{(1-\gamma D_{33})^2} \end{bmatrix}, \tag{36b}$$

where $\alpha = 2.0$ and $\gamma = 1.3$ are determined from the fit to experimental data for monotonic loading. For cyclic loading the unloading and reloading moduli (denoted as E_{u} and E_{r} respectively) are determined from the experimental results as below:

$$E_{\mathrm{u}} = \frac{1.3E_0}{1-\overline{D}}, \tag{37a}$$

$$E_{\mathrm{r}} = 1.1E_{\mathrm{u}}. \tag{37b}$$

It should be noted that in the unloading regime there will be no accumulation of damage. Whereas in reloading it keeps increasing to the stress point on the bounding surface of this circle with a speed given in Eqs. (29) and (30a,b) by replacing E_0 with E_{r} only.

4. Verification of the model

The theoretical formulations was examined by comparisons with experimental results. The experimental program included two primary loading configurations, namely triaxial monotonic and cyclic compressions. One nominal compressive strength of 10 ksi (69 MPa) was considered in the experimental program. The mix of the concrete is indicated in Table 1.

Table 1
Specimen mix proportions per cubic yard (m^3)

Design strength, ksi (MPa)	10 (69)
Concrete designation	HS10
Cement, lb. (kg)	768 (456)
Fly ash, lb. (kg)	0
Silica fume, lb. (kg)	92 (55)
Water, lb. (kg)	276 (164)
Aggregate, lb. (kg)	1690 (1001)
Sand, lb. (kg)	1298 (770)
High Range Water Reducer, l	2.6
Total weight, lb. (kg)	4110 (2438)
(w/cement) ratio	0.36
(w/cementitous) ratio	0.32

4.1. Testing procedure

The complete stress strain responses were obtained in a stiff frame servo-hydraulic closed loop testing system. The testing frame had a load capacity of 1000 kips (4600 KN). A microcomputer provided the command signals and dada for the closed-loop control of the experiments. A triaxial pressure vessel capable of applying a maximum confining pressure of 12,000 psi (83 MPa) on 4×8 in. (101×202 mm) cylindrical specimens was employed for triaxial tests. A confining pressure intensifier was used to fill and pressurize the triaxial cell and to provide servo-control of the confining fluid in the triaxial cell. In-vessel pressure and displacement transducers were applied for the control of the servo-valve through computer commands. The 4×8 in. (101×202 mm) cylindrical specimens were jacketed with a rubber membrane in order to prevent penetration of fluid into the specimen during pressurization. The confining effect of the rubber membrane on the axial stresses was examined by way of comparing the uniaxial compressive strengths of jacketed and bare specimens as an average 7% increase in axial strengths. The effect of rubber membrane on the axial strength of specimens was subsequently taken into account by this amount.

An in-vessel two-extensometer assembly with a gauge length of 2 in. was employed for measurements of axial strains. For the load path, the axial and confining pressures were simultaneously applied to the specimens at the rate of 4 ksi/min until the confining pressures reached the targeted values. At this point the confining pressure was kept constant at the target value. Then the axial stress was increased at a constant displacement rate of 0.00082 in./s (0.021 mm/s) for the triaxial monotonic compression (Fig. 3), whereas the

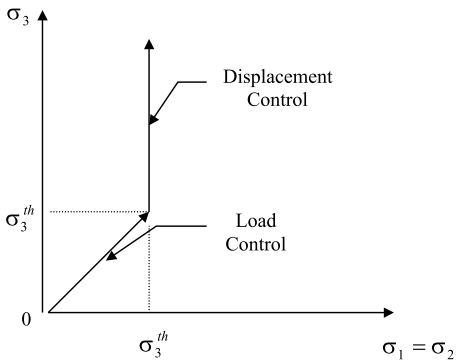

Fig. 3. Loading path.

axial stress was increased and decreased at a constant displacement rate of 0.00082 in./s (0.021 mm/s) every 0.02 in. (0.0508 mm) deformation for triaxial cyclic compression. A limited number of specimens were tested under cyclic loading conditions.

4.2. Experimental results

The failure strength, confinement ratio and strain ratio at failure for the high strength concrete specimens are given in Ansari and Li (1998). Average mechanical properties of the specimen in uniaxial tension and compression are given in Table 2. In this table, f'_c is the uniaxial compressive strength, v is the Poisson's ratio, E_0 refers to the modulus of elasticity in compression. Fitted parameter values of failure criterion are indicated in Table 3.

Theoretical and experimental stress strain relationships under triaxial monotonic and cyclic compressions are compared in Figs. 4 and 5 respectively. In Fig. 4, the two curves correspond to confining pressures of 2 ksi (14 MPa) and 10 ksi (69 MPa) respectively. It should be noted that the simulation for the initial stiffness of the second curve is not so good. The reason may be that this part corresponds to the higher hydrostatic compression, and the model may not predict its behavior very well. Fig. 5 corresponds to confining pressure of 2 ksi (14 MPa).

As shown in these figures, the results are in good agreement between the theoretical and experimental stress strain relationships.

5. Conclusions

The following conclusions are drawn based on the findings of this study:

1. The empirical failure criterion based on the four parameter model of Ottosen (1977) is valid also for high strength concrete.
2. The proposed bounding surface is able to portray the mechanism of damage in high strength concrete and therefore yields an appropriate constitutive model for the material in triaxial monotonic and cyclic compressions.

It is therefore possible to employ the constitutive relationship established here for the prediction of the stress strain response. Experimental evidence indicated good agreement between the theoretical model and

Table 2
Average mechanical properties of high strength concrete in compression

Specimen designation	HS10
f'_c, ksi	10.31
E_0, ksi	8.7×10^3
v	0.15

1 ksi = 6.895 MPa.

Table 3
Fitted parameter values of failure criterion

	A	B	k_1	k_2
HS10	15.9870	7.1636	10.218	6.2038

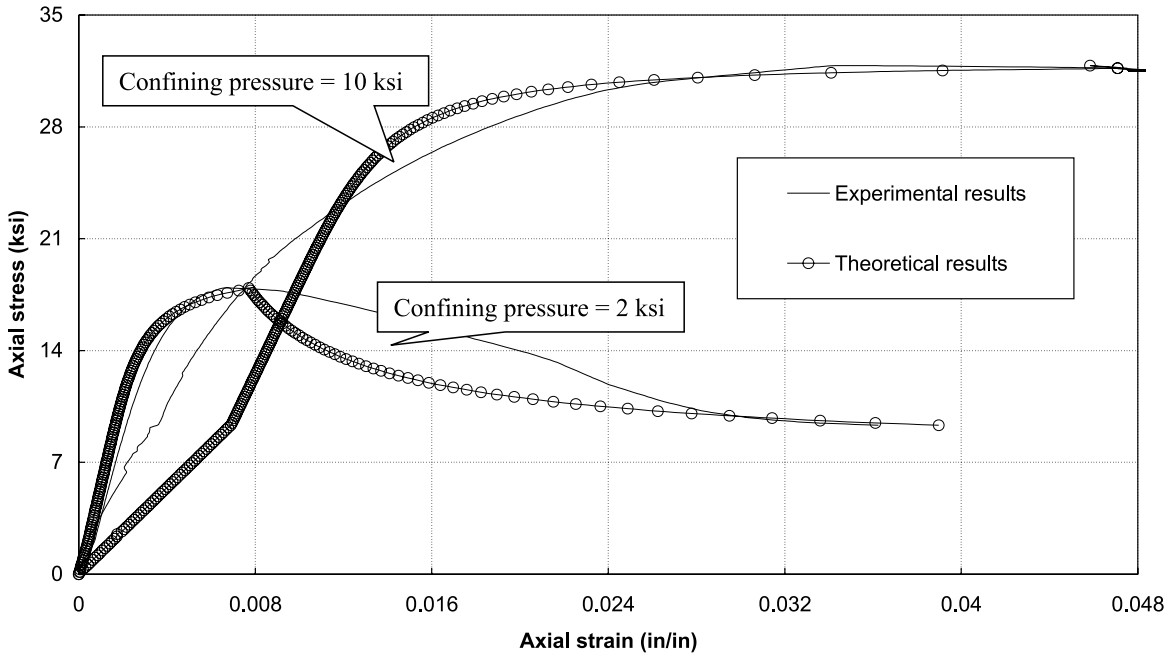

Fig. 4. Comparison of the theoretical and experimental stress strain relationships for 10 ksi (69 MPa) strength concrete in triaxial monotonic compression.

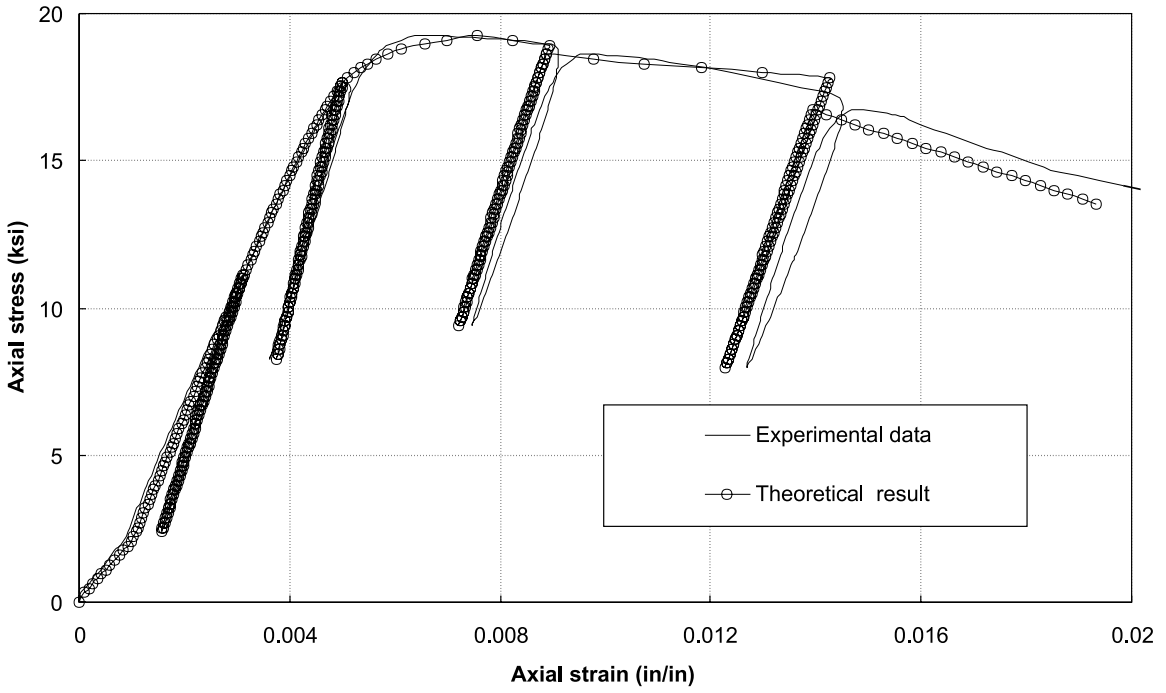

Fig. 5. Comparison of the theoretical and experimental stress strain relationships for 10 ksi (69 MPa) strength concrete in triaxial cyclic compression with confining pressure = 2 ksi (14 MPa).

the experimental stress strain relationships. However, data are still limited and more experimental results are required especially for the behavior under biaxial states of stress.

Acknowledgements

This work was performed under grants from the National Science Foundation (grant no. 59479027), the NSF of Yunnan Province (grant no. 98E004Z) and 985 project of Tsinghua University.

References

Ansari, F., Li, Q., 1998. High strength concrete subjected to triaxial compression. ACI Mater. J. 95 (6), 747–755.
Buyukozturk, O., Tseng, T.M., 1984. Concrete in biaxial cyclic compression. J. Struct. Eng. ASCE 110 (3), 461–476.
Cedolin, L., Crutzen, Y.R., Deipoli, S., 1977. Triaxial stress-strain relationship for concrete. J. Engrg. Mech. ASCE 103 (3), 423–439.
Chow, C.L., Wang, J., 1987. An anisotropic theory of elasticity for continuum damage mechanics. Int. J. Fract. 33, 3–16.
Dafalias, Y.F., 1986. Bounding surface plasticity, I: Mathematical foundation and hypoplasticity. J. Eng. Mech. 112 (9), 966–987.
Desai, C.S., Siriwardance, H.J., 1984. Constitutive Laws for Engineering Materials with emphasis on Geologic Materials. Prentice-Hall, Englewood Cliffs, NJ, pp. 344–403.
Fafitis, A., Shah, S.P., 1986. Constitutive model for biaxial cyclic loading of concrete. J. Eng. Mech. 112 (8), 760–775.
Fardis, M.N., Alibe, B., Tassoulas, J.L., 1983. Monotonic and cyclic constitutive law for concrete. J. Eng. Mech. ASCE 109 (2), 516–536.
Karsan, I.D., Jirsa, J.O., 1969. Behavior of concrete under compressive loading. J. Struct. Div. ASCE 95 (12), 2543–2563.
Kosovos, M.D., Newman, J.B., 1980. A mathematical description of performational behavior of concrete under generalized stress beyond ultimate strength. ACI J. 77 (5), 340–346.
Krajcinovic, D., Fonseka, G.U., 1981. The continuous damage theory of brittle materials. J. Appl. Mech. Trans. ASME 48, 809–824.
Krajcinovic, D., Selvaraj, S., 1983. Constitutive equations for concrete. In: Proceedings of International Conference On Constitutive Laws for Engineering Materials, Tuscon, Arizona, pp. 393–406.
Kupfer, H., Hilsdorf, H.K., Rusch, H., 1969. Behavior of concrete under biaxial stresses. ACI J. 66 (8), 656–666.
Li, Q.B., Ansari, F., 1999. Mechanics of damage and constitutive relationships for high strength concrete in triaxial compression. J. Eng. Mech. ASCE 125 (1), 1–10.
Mazars, J., 1986. Description of micro and macroscale damage of concrete structures. Engrg. Frac. Mech. 25 (5/6), 229–238.
Mazars, J., Cabot, G.P., 1989. Continuum damage theory—application to concrete. J. Eng. Mech. ASCE 115 (2), 345–365.
Ortiz, M., 1985. A constitutive theory for the inelastic behavior of concrete. Mech. Mater. 4 (1), 67–93.
Ottosen, N.S., 1977. Failure criterion for concrete. J. Eng. Mech. ASCE 103 (4), 527–535.
Voyiadjis, G.Z., Abu-Lebdeh, T.M., 1993. Damage model for concrete using bounding surface concept. J. Eng. Mech. 119 (9), 1865–1885.